AGU PUBLICATIONS

Geophysical Research Letters

RESEARCH LETTER
10.1002/2016GL068843

Key Points:
- The Illapel megathrust event reveals a two-stage rupture process with completely different slip characteristics
- The first stage built up energetically from deeper locked zone, and then the second stage ruptured slowly in the near trench area
- This unique rupture evolution is key to further in-depth study on earthquake physics and source dynamics of a subduction system

Supporting Information:
- Supporting Information S1
- Movie S1

Correspondence to:
S.-J. Lee,
sjlee@earth.sinica.edu.tw

Citation:
Lee, S.-J., T.-Y. Yeh, T.-C. Lin, Y.-Y. Lin, T.-R. A. Song, and B.-S. Huang (2016), Two-stage composite megathrust rupture of the 2015 M_w8.4 Illapel, Chile, earthquake identified by spectral-element inversion of teleseismic waves, *Geophys. Res. Lett.*, *43*, 4979–4985, doi:10.1002/2016GL068843.

Received 25 MAR 2016
Accepted 3 MAY 2016
Accepted article online 7 MAY 2016
Published online 27 MAY 2016

Two-stage composite megathrust rupture of the 2015 M_w8.4 Illapel, Chile, earthquake identified by spectral-element inversion of teleseismic waves

Shiann-Jong Lee[1], Te-Yang Yeh[1], Tzu-Chi Lin[2], Yen-Yu Lin[1], Teh-Ru Alex Song[3], and Bor-Shouh Huang[1]

[1]Institute of Earth Sciences, Academia Sinica, Taipei, Taiwan, [2]Institute of Geosciences, National Taiwan University, Taipei, Taiwan, [3]Department of Earth Sciences, University College London, London, UK

Abstract The M_w8.4 Illapel earthquake occurred on 16 September was the largest global event in 2015. This earthquake was not unexpected because the hypocenter was located in a seismic gap of the Peru-Chile subduction zone. However, the source model derived from 3-D spectral-element inversion of teleseismic waves reveals a distinct two-stage rupture process with completely different slip characteristics as a composite megathrust event. The two stages were temporally separated. Rupture in the first stage, with a moment magnitude of M_w8.32, built up energetically from the deeper locked zone and propagated in the updip direction toward the trench. Subsequently, the rupture of the second stage, with a magnitude of M_w8.08, mainly occurred in the shallow subduction zone with atypical repeating slip behavior. The unique spatial-temporal rupture evolution presented in this source model is key to further in-depth studies of earthquake physics and source dynamics in subduction systems.

1. Introduction

On 16 September 2015 at 22:54:32 (UTC), a large earthquake struck central Chile with a moment magnitude of M_w8.4. According to the United States Geological Survey (USGS) earthquake report, the hypocenter was located at 31.573°S, 71.674°W with a depth of 22.4 km, about 48 km west of Illapel, Chile (Figure 1), and 150 km north of Santiago, the capital of Chile. More than 60 aftershocks of magnitude greater than 5 were recorded within a month following the main shock. The Illapel earthquake also triggered tsunami waves that struck the coast of Chile within minutes. The shaking and tsunami caused 13 fatalities, 34 injuries while 6 remain missing, and thousands more were left homeless.

Based on the Global Centroid Moment Tensor (GCMT) inversion result, the faulting mechanism of the earthquake was interpreted as a reverse fault on a low-angle plane along the Peru-Chile Trench, where the Nazca Plate subducts beneath the South America Plate at a rate of 7–9 cm/yr [*DeMets et al*., 1990]. Previous studies have shown that numerous large earthquakes have struck different segments of South America margin with at least one *M*8+ event in each segment over the past 130 years [*Kelleher*, 1972; *Nishenko*, 1985]. In the segment where the Illapel earthquake occurred, both of the previous large events, including the 1960 M_w9.5 Valdivia earthquake [*Barrientos and Ward*, 1990] and the 2010 M_w8.8 Chile earthquake [*Lay et al*., 2010], occurred to the south of this event. Before the 2015 Illapel earthquake, there had been no events greater than magnitude 8 in the central Chile region (between 29°S and 32°S) since 1943. Part of the rupture zone of this earthquake coincides with that of the 1943 M_w8.2 Ovalle earthquake [*Beck et al*., 1998], the last large event that had occurred in this area.

Rapid analyses of the rupture process of the Illapel earthquake have been carried out [*Ye et al*., 2015; *Heidarzadeh et al*., 2016; *Melgar et al*., 2016]. These studies mostly used teleseismic, geodetic, or tsunami data to perform joint source inversions. However, as the geodetic observations were only conducted on the land-side, they provide weaker constraints on rupture information in the offshore area. In addition, the generation of a tsunami by a large earthquake is typically quite complex, which could be caused by coseismic seabed deformation or submarine landslides [*Kawamura et al*., 2012]. Thus, using tsunami data in a joint inversion may introduce bias into the results. In order to investigate the origin of this large earthquake and its relationship to the entire subduction system, a source inversion using global 3-D Green's functions based upon the spectral-element method (SEM) [*Komatitsch and Tromp*, 2002] was performed to image the fault slip to a 3-D subducting fault model [*Hayes et al*., 2012]. We used complete teleseismic (30–60°) and regional (0–30°) waveforms including *P* waves, *S* waves, reflections, and surface waves, in all *E*, *N*, and *Z* components. Two

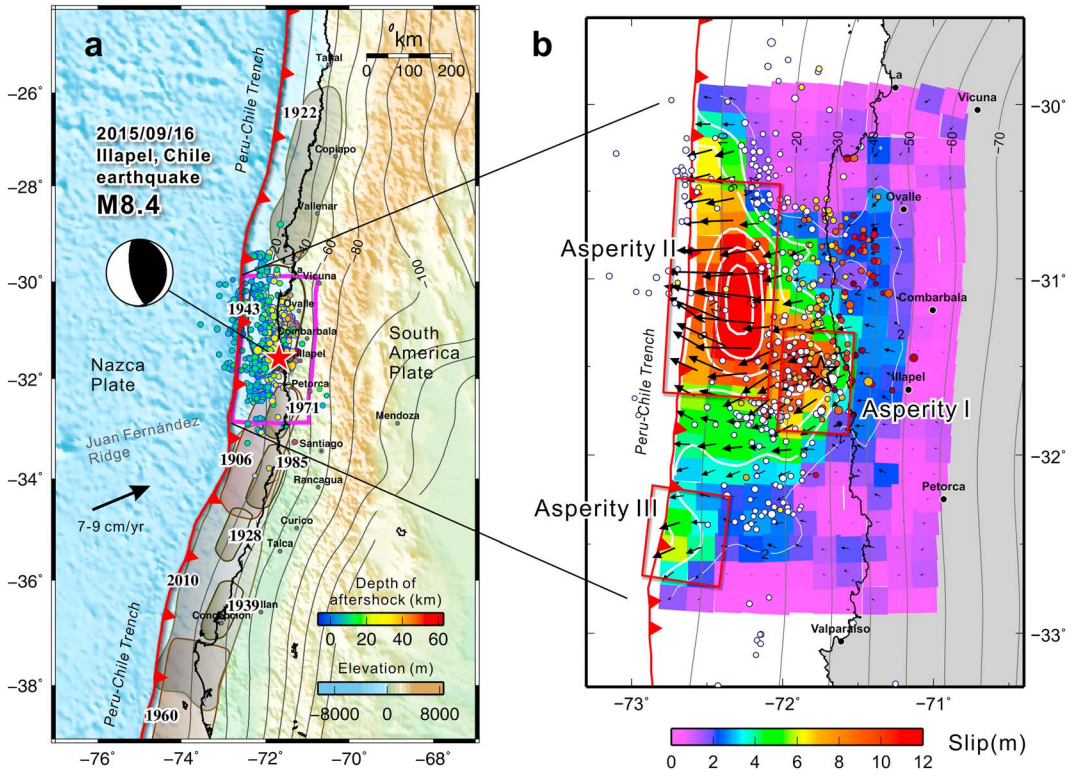

Figure 1. (a) Location map of the 16th September 2015 Illapel, Chile earthquake. Red star indicates the epicenter of the Illapel event. Locations of aftershocks occurred within 1 month after the main shock (taken from International Seismological Center earthquake catalog) are shown by colored circles. Beach ball shows the GCMT solution of the main shock. Rupture areas of the major subduction zone earthquakes are shown with gradient colors (referred to *Lay*, 2011). (b) Map of the slip distribution. The epicenter is indicated by a black star. Length and direction of the arrow at each subfault indicate the slip direction and the amount of slip, respectively. Warm colored circles indicate aftershocks in 1 month with magnitudes between 3.7 and 7.0.

passbands, 0.003–0.04 Hz and 0.003–0.02 Hz, were considered to serve as a joint inversion. A parallel nonnegative least squares inversion technique and a full time-space approach were applied to the inversion so as to flexibly represent the source time function of a complex rupture process [*Lee et al.*, 2011]. There are 100 time windows of 4 s in length set in the inversion, and each one has an overlap of 2 s. Thus, each subfault can slip by a flexible source time function within a time period of 202 s after the rupture front passes through. This large earthquake was well recorded by teleseismic stations worldwide which have good quality and sufficient azimuthal coverage around the source. In addition, full waveform inversion included constraints from body waves and surface waves which enables us to determine the fault rupture behavior accurately. Details about the inversion method and data processing are provided in the supporting information.

2. Spatial Slip Distribution

The slip distribution and corresponding waveform fits determined from source inversion are shown in Figures 1b and S1 in the supporting information, respectively. Inversion results show that the rupture mainly occurred in the shallow part of the subduction zone from the trench to 30 km depth. Three large slip areas with different slip characteristics can be found on the fault plane. One occurred at the deeper part around the hypocenter (Asperity I). The slip in this area was predominately reverse orientation with right-lateral thrust motion. The maximum slip in Asperity I was around 10 m. The second asperity developed in the northern shallow fault plane close to the trench (Asperity II). This asperity is the largest with a size of about 130 km along the strike direction and 50 km in the downdip direction. The movement type varied from pure thrust in the northern part to thrust with some left-lateral motion in the southern part of Asperity II. Slip in this asperity reached up to 16 m. Finally, a slip patch (Asperity III) with oblique (right-lateral) thrust motion and a relatively smaller slip of 6 m were located in the southern shallow fault plane. The rupture near the southernmost slip

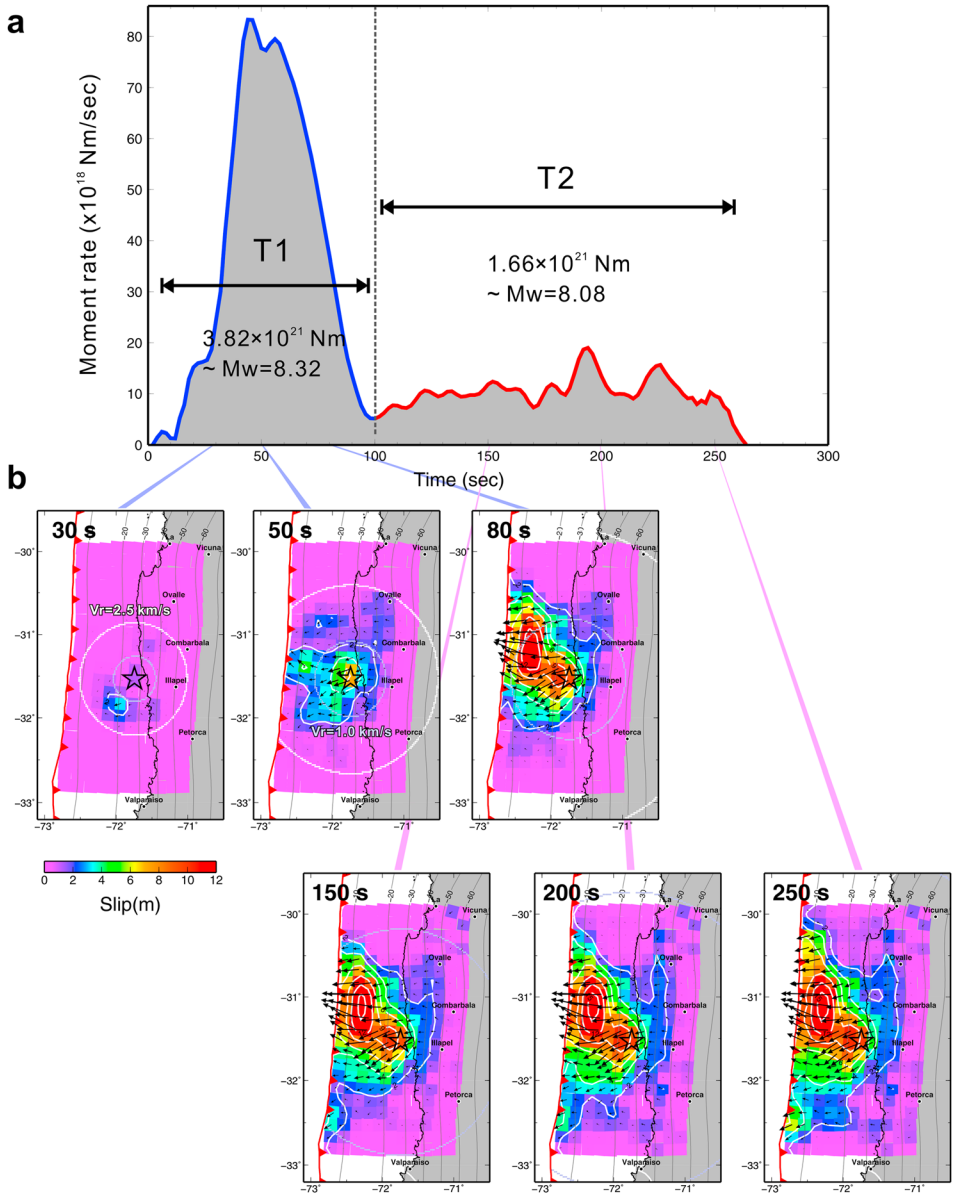

Figure 2. Moment rate function and rupture snapshots. (a) Moment rate of the Illapel earthquake. The two time periods of moment release, i.e., T1 and T2, are separated by the dotted line. Seismic moment for each individual time period and the equivalent moment magnitude are shown. (b) Accumulated slip as a function of time is shown in the panels from left to right. The dotted open circles indicate two reference rupture fronts of $V_r = 2.5$ km/s and $V_r = 1.0$ km/s, respectively. (see also Movie S1).

zones halted at around 33°S, where the Juan Fernández Ridge is subducting into the Peru-Chile Trench [*Huene et al.*, 1997].

The aftershocks mostly occurred around the boundaries of these large slip areas, and almost no aftershocks with $M > 6$ were found inside Asperity II or Asperity III (Figure 1b). This implies that the stress in these areas had been completely released during the rupture of main shock. A large number of deep aftershocks occurred close to Asperity I near the hypocenter. Some deep aftershocks with depths of around 30 to 40 km could also be observed north of the hypocenter, where relatively small slip occurred during the main shock.

3. Temporal Rupture Process

Snapshots of the rupture process are shown in Figure 2 (An animation of rupture process is provided in the Movie S1). Short slip pulses can be found near the southwest of hypocenter during the first 30 s of rupture.

The slip reached around 6 m between 30 and 50 s at the deeper part of the subduction zone, close to the hypocenter that formed the first asperity (Asperity I). Then the rupture quickly propagated toward the updip direction and extended to the shallow subduction zone. Here rupture occurred over a broad region and lasted from 50 to about 90 s which formed the main slip area of Asperity II. There is no resolvable slip for the next 5–10 s. Following this quiet period, the fault moved again when the shallow subduction zone started to slip in several sparse areas. The rupture developed in the south and north along the trench from 100 to approximately 250 s. A large amount of slip accumulated in the northern shallow fault plane, rerupturing the area that slipped from 50 to 90 s. This area continued slipping for a very long time and became the largest asperity (Asperity II). Between 100 and 250 s, rupture also developed in the shallow subduction zone toward the south, where the fault slipped slowly and gradually formed the latest asperity (Asperity III). Before the end of the rupture, small slip patches occurred in the deeper fault plane north of the hypocenter. The fault movement gradually stopped, and no significant slip occurred after 250 s.

Two reference rupture fronts with rupture velocities (V_r) of 2.5 km/s and 1.0 km/s are shown in Figure 2b (see also Movie S1). All the large slip bracketed by the two rupture fronts occurred during the first 100 s. This implies that the rupture speed was relatively low ($V_r < 2.5$ km/s), slower than 80% of the shear wave speed during this time period. After the first 100 s, when the slip started to develop in the shallow subduction zone, it lagged behind the two reference rupture fronts. The rupture velocity for the slip developed along the trench was lower than 1.0 km/s in this time period.

From the temporal rupture snapshots, it appears that the Illapel earthquake involved a two-stage rupture process. This phenomenon is even clearer when the moment rate function is examined. Two separated peaks of moment release can be identified (Figure 2a). The first peak lasted from 0 to 100 s (T1), starting with a small peak at the beginning (0 ~ 10 s), followed by an energetic moment release with a very large peak at around 45 s and continuing to about 100 s. The second energy release occurred from 100 to about 250 s (T2). It had a longer duration than that of T1 and contained several small peaks. Between T1 and T2, there was very little moment release. This is consistent with the snapshot showing a quiet period at around 100 s.

The moment rate function with the rupture snapshots indicate that the time period T1 was related to the initial slip near the hypocenter and subsequently ruptured updip. This time period included the developments of Asperity I and the main slip of Asperity II. The energy release in the second time period (T2) was mostly related to the fault slip in the shallow subduction zone along the trench. This time period included the further growth of the biggest asperity (Asperity II) at the northern subduction zone and a smaller asperity (Asperity III) at the southern fault plane. We note that the slip in T2 was a collection of spatially and temporally sparse slip patches and thus released less coherent radiated energy to seismic waveforms. These features are obvious in snapshots of slip (Movie S1) and the source time function (Figure 2). Combining these two time periods together, the overall rupture duration time was around 250 s for a total seismic moment of 5.48×10^{21} Nm, which is equivalent to an earthquake of M_w8.43. The estimated average stress drop is 3.34 MPa, which is close to published values of interplate earthquakes [*Kanamori and Anderson*, 1975].

4. Discussion

Two separate time periods of energy release were found from the inversion result, whereas previously published models [*Ye et al*., 2015; *Heidarzadeh et al*., 2016; *Melgar et al*., 2016] suggest that the rupture mostly terminated after the first 100 s. Assuming that the two-stage rupture is fairly close to that of the Illapel earthquake, this model can generally recover as many observations as possible, especially observations at regional distances. In order to clarify this issue, we performed two 3-D SEM global seismic wave propagation simulations based on two different rupture models. One was taken from the source inversion result with a single-stage rupture process (Model 1, see supporting information and Figure S2), and the other was based on this source inversion result, which contains two stages of rupture (Model 2). A comparison of waveforms determined from these two simulations is shown in Figure S3. The test results indicate that the simulation based on Model 2 can reproduce the observed waveforms for both low- and high-frequency bands significantly better. For the high-frequency signals, the two-stage model mostly improved the amplitudes and timings of the body waves. Some regional stations show complex high-frequency signals, such as TRQA and COYC. These high-frequency phases caused from complex source rupture process can only be simulated by Model 2. The low-frequency signals also had better fits with Model 2, especially in the phase time and envelope

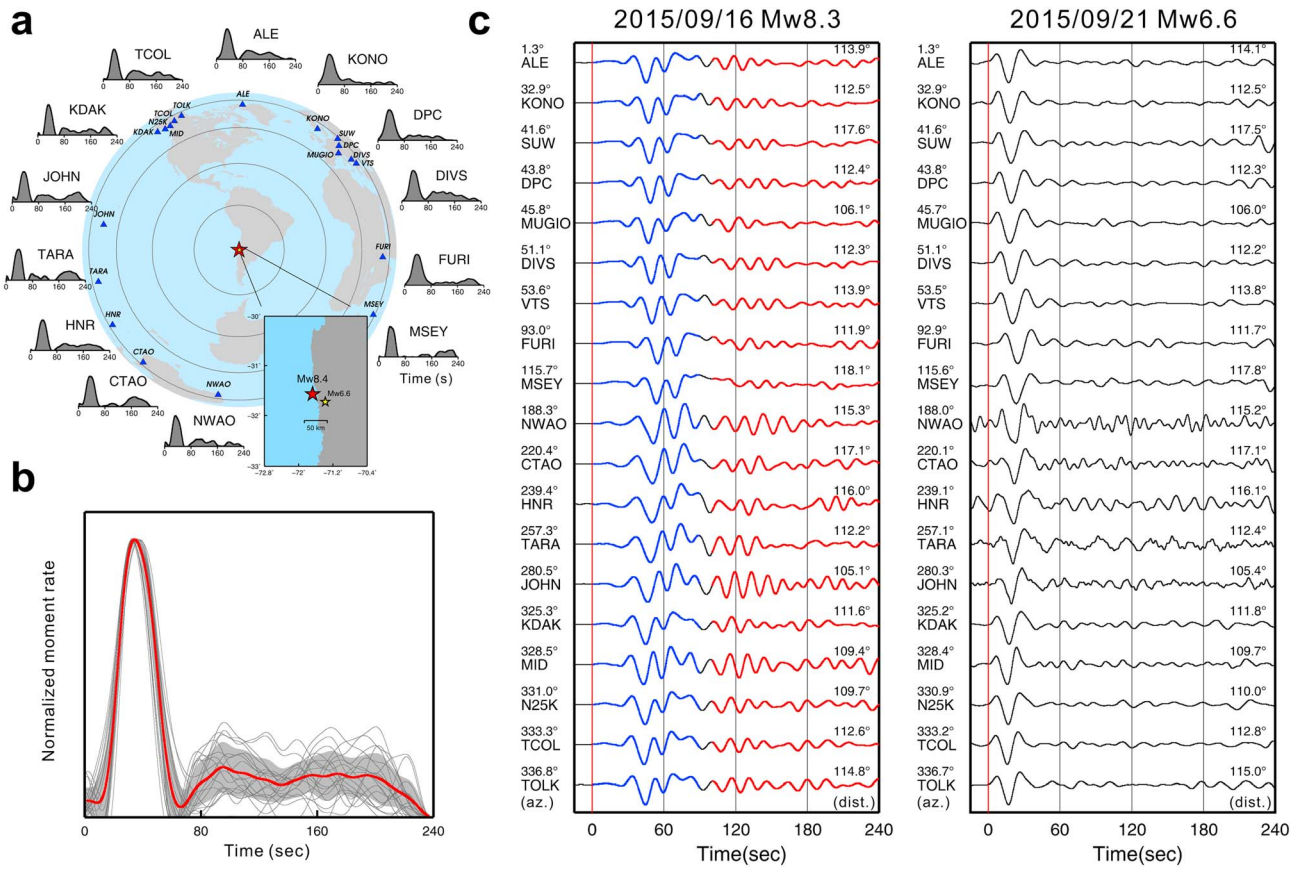

Figure 3. Source time function estimated from Pdiff records by the EGF analysis. (a) Locations of stations at which Pdiff phases were recorded and RSTFs estimated at each station. (b) Normalized RSTFs (gray thin lines) and the averaged RSTF (red thick line) with uncertainty of 1 standard deviation (denoted by gray band). (c) Comparisons of Pdiff record sections of the 2015 M_w8.4 Illapel, Chile, earthquake and a smaller event (the 21 September 2015 M_w6.6 aftershock) which used as EGFs. Records are sorted by azimuths in an ascending order. Stage I and stage II segments are, respectively, colored by blue and red.

shape of the surface waves. It is noted that some higher-frequency wiggles embedded in the surface waves can be found in regional broadband seismograms, for example, EFI, SPB, and SAML. These signals might correspond to the slip in the second stage where complex ruptures developed in the shallow subduction zone that produced stronger surface wave energy. Again, these wiggles can be explained by Model 2 but cannot be fit by Model 1. A misfit function, defined as $(A-b)^2/b^2$ where A is the forward synthetic and b is the observation, is used to evaluate the quality of waveform fitting. In the frequency bands of 0.003 to 0.04 Hz and 0.003 to 0.02 Hz, the waveform misfits for Model 1 and Model 2 are 0.319 and 0.119, respectively.

To further examine the validity of the proposed two-stage rupture model, we performed an empirical Green's function (EGF) deconvolution of Pdiff waves (see supporting information) to estimate the relative source-time functions (RSTFs) of the Illapel earthquake. In the Pdiff record section (Figure 3c), the stage II contribution (marked in red) are featured by several strong amplitudes with durations of at least 140 s following the end of stage I (marked in blue). To ensure that the later strong phases were attributed to the stage II source rupture, we compare the same Pdiff record section of an M_w6.6 aftershock (21 September 2015, 17:40:00 UTC). Unlike the case for the M_w8.4 event, it is clear that no significant strong later phases can be found following the source phases of the small event (Figure 3c). We use the Pdiff waveforms of the M_w6.6 event as EGFs. The RSTFs estimated in different azimuths consistently show an energetic first stage followed by a gentle second stage with a longer duration (Figures 3a and 3b). The characteristics of the stacked RSTFs are comparable with the moment rate function derived from the finite fault inversion. The EGF deconvolution analysis of another M_w6.1 aftershock (21 September 2015, 05:39:34 UTC) also showed a similar result (see Text S5). Note that the M_w6.6 event was not beneath the ocean, whereas the M_w6.1 event was shallower in offshore closing to the trench. With the independent evidence from

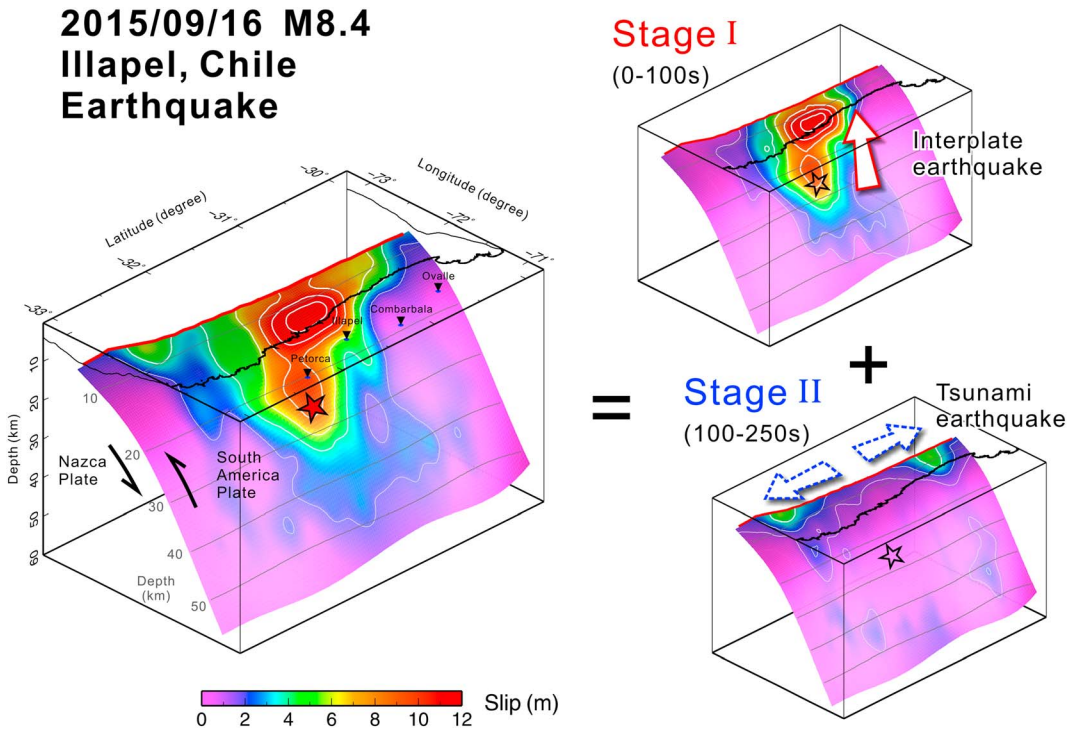

Figure 4. Schematic interpretation of the two-stage composite megathrust slip. The slip areas that occurred between 0 to 100 s and 100 to 250 s are mapped onto the 3-D slab model for rupture stage I and rupture stage II, respectively. The arrows show the main directions of rupture propagation in the different stages.

the Pdiff observations, the two-stage rupture model with a rupture duration over 200 s is probably a reasonable estimation of the actual source model of the Illapel event.

To clearly demonstrate the two-stage energy release model, the slip distribution was further decomposed into contributions from stage I and stage II, separately (Figure 4). The first stage ruptured from the hypocenter in the updip direction. Similar to the 1995 Jalisco earthquake [*Ammon*, 1997] and the 2008 Tonga earthquake, this stage is therefore considered to be a typical interplate earthquake that mostly ruptures the deeper locked zone and the intermediate depth region (10 to 30 km depth) between two plates. The seismic moment of this stage is 3.82×10^{21} Nm, equivalent to an M_w8.32 earthquake. Conversely, the rupture of the second stage occurred in a broad area of the shallow subduction zone. Since it ruptured along the trench region with a slow rupture speed, the process in this stage is more likely a tsunami earthquake [*Kanamori*, 1972]. Some other events share similar characteristics, for example, the 2006 Java tsunami earthquake. The seismic moment of this stage is 1.66×10^{21} Nm, equivalent to an M_w8.08 earthquake. Due to the smaller moment release, the second stage may contribute less to the total tsunami excitation, compared to that from the first stage. The moment magnitude of the two-stage model is M_w8.43, which is larger than that in the earthquake report from the USGS (M_w8.3) but closer to that of the teleseismic and tsunami analyses [*Heidarzadeh et al.*, 2016], which resulted in a value of M_w8.4.

It is worth noting that slip occurred repeatedly at shallower subfaults where the second stage rupture was found. This is evidenced by multiple-peak slip rate function in the shallow fault plane (Figure S5). Repetitions of rupture have been found in other large megathrust events. One comparable example is the occurrences of large-scale repeating slip patches during the 2011 Tohoku-Oki earthquake, which were found at the region shallower than the hypocenter [*Lee et al.*, 2011; *Galvez et al.*, 2016]. On the contrary, subfaults at a deeper fault plane radiated more short period energy, especially at the beginning of the rupture. This shorter period characteristic observed in the Illapel earthquake is also consistent with the findings from the Tohoku-Oki Earthquake [*Simons et al.*, 2011], which shows that sources of high-frequency seismic waves delineate the edges of the deepest portions of the coseismic slip.

There are several plausible explanations for the two-stage rupture process. One possible reason is that the stress state immediately changed after the first rupture stage. Stress condition at the shallower part of the

subducting interface therefore became critical, so that weak extra loading can lead to dynamic rupture propagation along the trench [*Ripperger et al*., 2007]. The second possibility is that the slip might rebound from the free surface of the fault, i.e., the trench. This rebounded rupture behavior is similar to one of the source models of the Tohoku-Oki earthquake [*Ide et al*., 2011]. Third, the second stage rupture can be considered as a rapid postseismic slip. Although postseismic slip usually occurs within days or months of the main shock, part of the postseismic slip may also occur shortly following the main shock [*Miyazaki and Larson*, 2008].

5. Conclusions

In summary, a two-stage rupture process was found during the Illapel earthquake. The first stage originated from the hypocenter then ruptured in an updip direction to the shallow fault plane, and the second stage developed in the shallow subduction zone that ruptured slowly along the trench. This model was verified by forward global wave propagation simulations and direct evidence from teleseismic Pdiff records. From these results, we concluded that the two-stage rupture process would be the main source characteristic of the Illapel earthquake. The result is crucial for the determination of strain budget along the Peru-Chile Trench since stress interaction may occur with the adjacent trench segments. In particular, the segment to the north of this event demonstrates similar seismic gap since the 1922 event. Now, further questions remain. What is the dynamic mechanism that causes this two-stage rupture phenomenon? Is it a natural state that occurs frequently in subduction zone earthquakes? To answer these questions, high-resolution kinematic source models will be crucial for further investigation of the dynamic properties, not only for megathrust events but also for the whole subduction process.

Acknowledgments
We thank Kuo-Fong Ma and Hiroo Kanamori for fruitful discussions and suggestions. Comments and suggestions by two anonymous reviewers were very helpful for improving the manuscript. The teleseismic data used were obtained from Incorporated Research Institutions for Seismology (IRIS). This research was supported by Academia Sinica and funded through the Taiwan Numerical Earthquake Model (TNEM) project (grant 102-Investigator Award-02). This research was also supported by the Taiwan Earthquake Research Center and funded through the Ministry of Science and Technology (grant MOST 103-2628-M-001-004-MY3). TEC contribution number for this article is 00122.

References

Ammon, C. J. (1997), The 1995 Colima-Jalisco, Mexico, earthquake (M_w8): A study of the rupture process, *Geophys. Res. Lett.*, *24*, 1019–1022, doi:10.1029/97GL00945.

Barrientos, S. E., and S. N. Ward (1990), The 1960 Chile earthquake: Inversion for slip distribution from surface deformation, *Geophys. J. Int.*, *103*(3), 589–598.

Beck, S., S. Barrientos, E. Kausel, and M. Reyes (1998), Source characteristics of historic earthquakes along the central Chile subduction Askew et Alzone, *J. South Am. Earth Sci.*, *11*, 115–129.

DeMets, C., R. G. Gordon, D. F. Argus, and S. Stein (1990), Current plate motions, *Geophys. J. Int.*, *101*, 425–478.

Galvez, P., L. A. Dalguer, J. P. Ampuero, and D. Giardini (2016), Slip reactivation during the 2011 M_w 9.0 Tohoku earthquake: Dynamic rupture and ground motion simulations, *Bull. Seismo. Soc. Am.*, in press.

Hayes, G. P., D. J. Wald, and R. L. Johnson (2012), Slab1. 0: A three-dimensional model of global subduction zone geometries, *J. Geophys. Res.*, *117*, B01302, doi:10.1029/2011JB008524.

Heidarzadeh, M., S. Murotani, K. Satake,T. Ishibe, and A. R. Gusman (2016), Source model of the 16 September 2015 Illapel, Chile, M_w 8.4 earthquake based on teleseismic and tsunami data, *Geophys. Res. Lett.*, *43*, doi:10.1002/2015GL067297.

Huene, R. V., J. Corvalán, E. R. Flueh, K. Hinz, J. Korstgard, C. R. Ranero, and W. Weinrebe (1997), Tectonic control of the subducting Juan Fernández Ridge on the Andean margin near Valparaiso, Chile, *Tectonics*, *16*, 474–488, doi:10.1029/96TC03703.

Ide, S., A. Baltay, and G. C. Beroza (2011), Shallow dynamic overshoot and energetic deep rupture in the 2011 M_w9.0 Tohoku-Oki earthquake, *Science*, *332*(6036), 1426–1429.

Kanamori, H. (1972), Mechanism of tsunami earthquakes, *Phys. Earth Planet. Inter.*, *6*, 346–359.

Kanamori, H., and D. L. Anderson (1975), Theoretical basis of some empirical relations in seismology, *Bull. Seismol. Soc. Am.*, *65*, 1073–1095.

Kawamura, K., T. Sasaki, T. Kanamatsu, A. Sakaguchi, and Y. Ogawa (2012), Large submarine landslides in the Japan Trench: A new scenario for additional tsunami generation, *Geophys. Res. Lett.*, *39*, L05308, doi:10.1029/2011GL050661.

Kelleher, J. A. (1972), Rupture zones of large South American earthquakes and some predictions, *J. Geophys. Res.*, *77*, 2087–2103, doi:10.1029/JB077i011p02087.

Komatitsch, D., and J. Tromp (2002), Spectral-element simulations of global seismic wave propagation—II. Three-dimensional models, oceans, rotation and self-gravitation, *Geophys. J. Int.*, *150*, 303–318.

Lay, T., C. J. Ammon, H. Kanamori, K. D. Koper, O. Sufri, and A. R. Hutko (2010), Teleseismic inversion for rupture process of the 27 February 2010 Chile (M_w8.8) earthquake, *Geophys. Res. Lett.*, *37*, L13301, doi:10.1029/2010GL043379.

Lay, T. (2011), Earthquakes: A Chilean surprise, *Nature*, *471*, 174–175.

Lee, S. J., B. S. Huang, M. Ando, H. C. Chiu, and J. H. Wang (2011), Evidence of large scale repeating slip during the 2011 Tohoku-Oki earthquake, *Geophys. Res. Lett.*, *38*, L19306, doi:10.1029/2011GL049580.

Melgar, D., W. Fan, S. Riquelme, J. Geng,C. Liang, M. Fuentes, G. Vargas, R. M. Allen, P. M. Shearer, and E. J. Fielding (2016), Slip segmentation and slow rupture to the trench during the 2015, M_w8.3 Illapel, Chile earthquake, *Geophys. Res. Lett.*, *43*, 961–966, doi:10.1002/2015GL067369.

Miyazaki, S. I., and K. M. Larson (2008), Coseismic and early postseismic slip for the 2003 Tokachi-oki earthquake sequence inferred from GPS data, *Geophys. Res. Lett.*, *35*, L04302, doi:10.1029/2007GL032309.

Nishenko, S. P. (1985), Seismic potential for large and great interplate earthquakes along the Chilean and southern Peruvian margins of South America: A quantitative reappraisal, *J. Geophys. Res.*, *90*, 3589–3615, doi:10.1029/JB090iB05p03589.

Ripperger, J., J. P. Ampuero, P. M. Mai, and D. Giardini (2007), Earthquake source characteristics from dynamic rupture with constrained stochastic fault stress, *J. Geophys. Res.*, *112*, B04311, doi:10.1029/2006JB004515.

Simons, M., et al. (2011), The 2011 magnitude 9.0 Tohoku-Oki earthquake: Mosaicking the megathrust from seconds to centuries, *Science*, *332*(6036), 1421–1425.

Ye, L. L., T. Lay, H. Kanamori, and K. Koper (2015), Rapidly estimated seismic source parameters for the 16 September 2015 Illapel, Chile M_w8.3 earthquake, *Pure Appl. Geophys.*, doi:10.1007/s00024-015-1202-y.